

DOI: 10.1002/adma.200703188

Nanostructured ZnS:Ni²⁺ Photocatalysts Prepared by Ultrasonic Spray Pyrolysis**

By Jin Ho Bang, Richard J. Helmich, and Kenneth S. Suslick*

Zinc sulfide (ZnS) has found diverse applications as optical phosphors, catalysts, photonic crystals, and light-emitting materials.^[1] In addition, ZnS has been examined as a photocatalyst, in part because of its high energy conversion efficiency and the relatively negative redox potential of its conduction band.^[1c,d] As a photocatalyst, ZnS has been examined for degradation of water pollutants, reduction of toxic heavy metals, and water-splitting for H₂ evolution.^[2] Owing to its large bandgap (3.6 eV), ZnS itself absorbs only in the UV, but its absorbance can be easily tuned by doping with metal ions, including Mn,^[1b,1f] Ni,^[2c] Cu,^[2d] and Pb.^[2e] In addition, the optical properties of ZnS strongly depend on particle size and morphology.^[3] Our ability, however, to control simply and systematically the crystal structure, solid morphology, and photoreactivity remains limited. Here we report a facile preparation of nanostructured Ni²⁺-doped ZnS (ZnS:Ni²⁺) hollow microspheres and nanoparticles by using ultrasonic spray pyrolysis (USP). Further, we find that our ZnS:Ni²⁺ nanoparticles are active and stable for photocatalytic H₂ evolution from aqueous K₂SO₃ and Na₂S solution under visible light owing to their excellent crystallinity and high surface area compared to traditional ZnS:Ni²⁺ powders.

USP is a robust synthetic method^[4–6] and has been used to produce a diverse range of nanostructured materials, including metal chalcogenide quantum dots,^[5b] metal oxides,^[6] carbon,^[6] and others. The preparation of ZnS:Ni²⁺ hollow microspheres and nanoparticles using USP is illustrated in Figure 1 (cf. Supporting Information (SI) for further description of the USP apparatus). An aerosol of the precursor solution (e.g., 200 mM Zn(NO₃)₂, 1 M thiourea, and 0.2 mM Ni(NO₃)₂ in water with 3% colloidal silica) was generated by ultrasonic nebulization, and the resulting mist was carried through a heated zone (700 °C) by an inert gas (Ar) flow.

As water rapidly evaporates, ZnS starts to precipitate at the droplet surface, solvent evaporates, and decomposition gases (e.g., NO_x, NH₃, HNCS) are evolved. Owing to the relatively low solubility of ZnS and its precursors, the decomposition of the droplet leads to an outer shell enriched in ZnS with a core of primarily silica particles. When the silica template was dissolved using an ethanolic HF solution, nanostructured ZnS:Ni²⁺ mesoporous hollow microspheres were obtained (Fig. 2a and b; see further scanning electron microscopy (SEM) and transmission electron microscopy (TEM) analyses in SI).

When the furnace temperature was increased from 700 °C to 1000 °C, however, the final product after HF treatment consisted of agglomerated nanoparticles (i.e., the microspheres lost structural integrity; Fig. 2c and d; see further SEM and TEM analyses in SI). As a control experiment, when the same precursor solution without the silica colloid template was nebulized and passed through the tube furnace at 1000 °C under Ar flow, only micrometer-sized solid microspheres of ZnS:Ni²⁺ were obtained, as shown in Figure 2e and f.

Figure 3 shows the diffuse reflectance UV-vis spectra and powder X-ray diffraction (XRD) patterns of ZnS:Ni²⁺ hollow microspheres, nanoparticles, and solid microspheres, respectively. The UV-vis spectra of all three morphologies of the ZnS:Ni²⁺ show a broad absorbance in the visible region, extending to ca. 550 nm as compared to non-doped ZnS (dashed line), indicating that doped Ni²⁺ forms a new energy level in the band structure of ZnS.^[2c] Higher-temperature processing increases the relative intensity of the absorbance from the Ni²⁺-doping and also the apparent crystallite size: as determined by the peak widths in the XRD patterns using the Debye–Scherrer equation, the crystallite sizes for the hollow microspheres, the nanoparticles, and the non-templated solid microspheres are 7.3 nm, 27 nm, and >50 nm, respectively. These calculated crystallite sizes are in good agreement with direct TEM observations (Fig. S10 in SI). In all cases, the ZnS:Ni²⁺ shows a hexagonal wurtzite structure (which is thermodynamically favored at high temperatures.^[1b,7]) in the XRD, which is confirmed by high-resolution TEM observation and selected-area electron diffraction (SAED) patterns, as shown in Figure 4. The hollow microspheres show broad diffraction peaks due to smaller crystallite size; owing to the width of the XRD peaks and the close overlap of the hexagonal wurtzite and cubic zinc blende structures, we cannot definitively rule out the presence of some zinc blende structure in the hollow microspheres.

Pore structures and size distributions of ZnS:Ni²⁺ were examined by N₂ adsorption/desorption isotherms (Fig. S9 in

[*] Prof. K. S. Suslick, J. H. Bang, R. J. Helmich
School of Chemical Sciences
University of Illinois at Urbana-Champaign
600 South Mathews Avenue, Urbana, IL 61801 (USA)
E-mail: ksuslick@uiuc.edu

[**] This material is based on work supported by the U.S. Department of Energy, Division of Materials Sciences under Award No. DE-FG02-07ER46418, through the Frederick Seitz Materials Research Laboratory at the University of Illinois at Urbana-Champaign. This research was carried out in part in the Center for Microanalysis of Materials, UIUC, which is partially supported by the U.S. Department of Energy under grant DE-FG02-07ER46418. Supporting Information is available online from Wiley InterScience or from the authors.

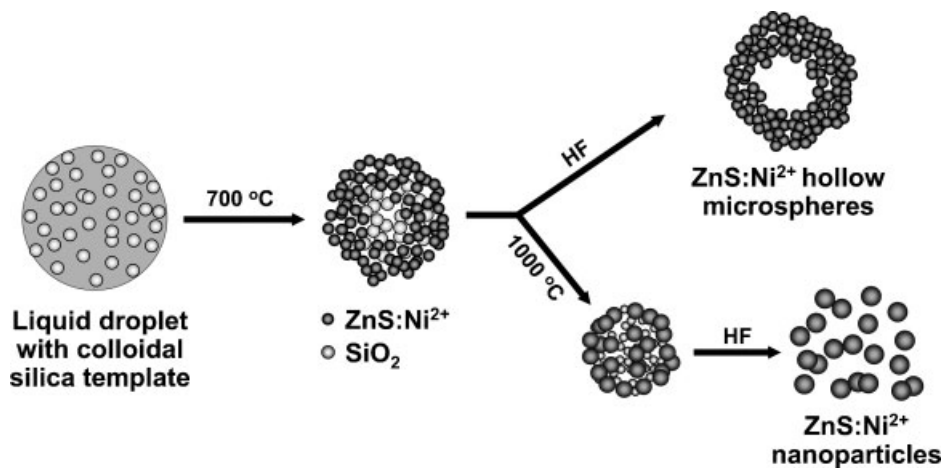


Figure 1. Schematic of the ultrasonic spray pyrolysis (USP) synthesis of hollow microspheres and nanoparticles of Ni²⁺-doped ZnS.

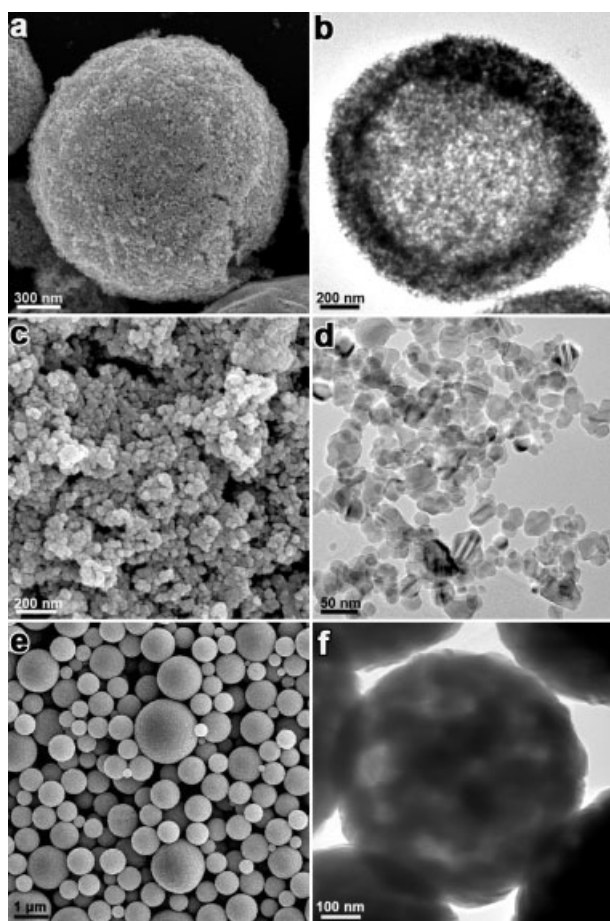


Figure 2. SEM and TEM images of nanostructured ZnS:Ni²⁺ hollow microspheres (a and b, respectively), nanoparticles (c and d, respectively), and non-templated solid microspheres (e and f, respectively).

SI). The Brunauer–Emmett–Teller (BET) surface areas of the hollow microspheres, the nanoparticles, and the non-templated solid microspheres are, respectively, 102 m² g⁻¹, 47 m² g⁻¹ (probably due to the larger crystallites of the higher temperature processing), and 2.0 m² g⁻¹. The hollow microspheres show a typical type-IV isotherm, characteristic of mesoporous materials, with a narrow and uniform pore size distribution centered at 23 nm, which corresponds to the size of silica colloid used in this synthesis.

The formation of the hollow microspheres made up of small nanoparticles is temperature-dependent: at 700 °C, a rigid mesoporous network of ca. 7 nm nanoparticles is formed, whereas at 1000 °C, the structural integrity of the micro-

sphere is lost and agglomerated nanoparticles are isolated instead. This is probably due to rapid crystal growth of ZnS at high temperatures;^[1b] this results in larger ZnS nanoparticles (ca. 27 nm, which are larger than the silica colloid template) that are not sufficiently strongly held together to sustain the hollow microsphere structure after the silica template is removed. In addition to the rapid crystal growth, gas released during the decomposition of the ZnS precursors may also lead to the destruction of the porous microspheres, as noted in other systems.^[8]

Metal sulfides such as CdS^[9a] and solid solution ZnS-CuInS₂-AgInS₂^[9b,c] have been extensively investigated as a visible-light-driven photocatalysts because of their relatively narrow bandgaps and relatively high quantum efficiencies. Simple ZnS doped with various metal ions has also been examined as a photocatalyst for water-splitting, but generally more limited quantum efficiencies have been reported.^[2]

We have examined visible light photocatalytic water-splitting from our ZnS:Ni²⁺ systems in the presence of sacrificial electron donors (K₂SO₃ and Na₂S) and made quantitative comparisons between the hollow spheres, nanoparticles, and solid spheres. Figure 5a shows a comparison on the amounts of H₂ produced photocatalytically by ZnS:Ni²⁺ hollow microspheres, nanoparticles, and solid spheres without the use of a co-catalyst (e.g., Pt nanoparticles). The most efficient of these are ZnS:Ni²⁺ nanoparticles, in spite of the much larger surface area of the ZnS:Ni²⁺ hollow microspheres. The low activity of the hollow spheres is probably related to the small crystallite or poor crystallinity of small nanoparticles that make up the hollow spheres because electron-hole recombination mainly occurs at surface defect sites.^[10] Despite their better crystallinity, the solid microspheres also show a lower activity than the nanoparticles, which is attributed to their

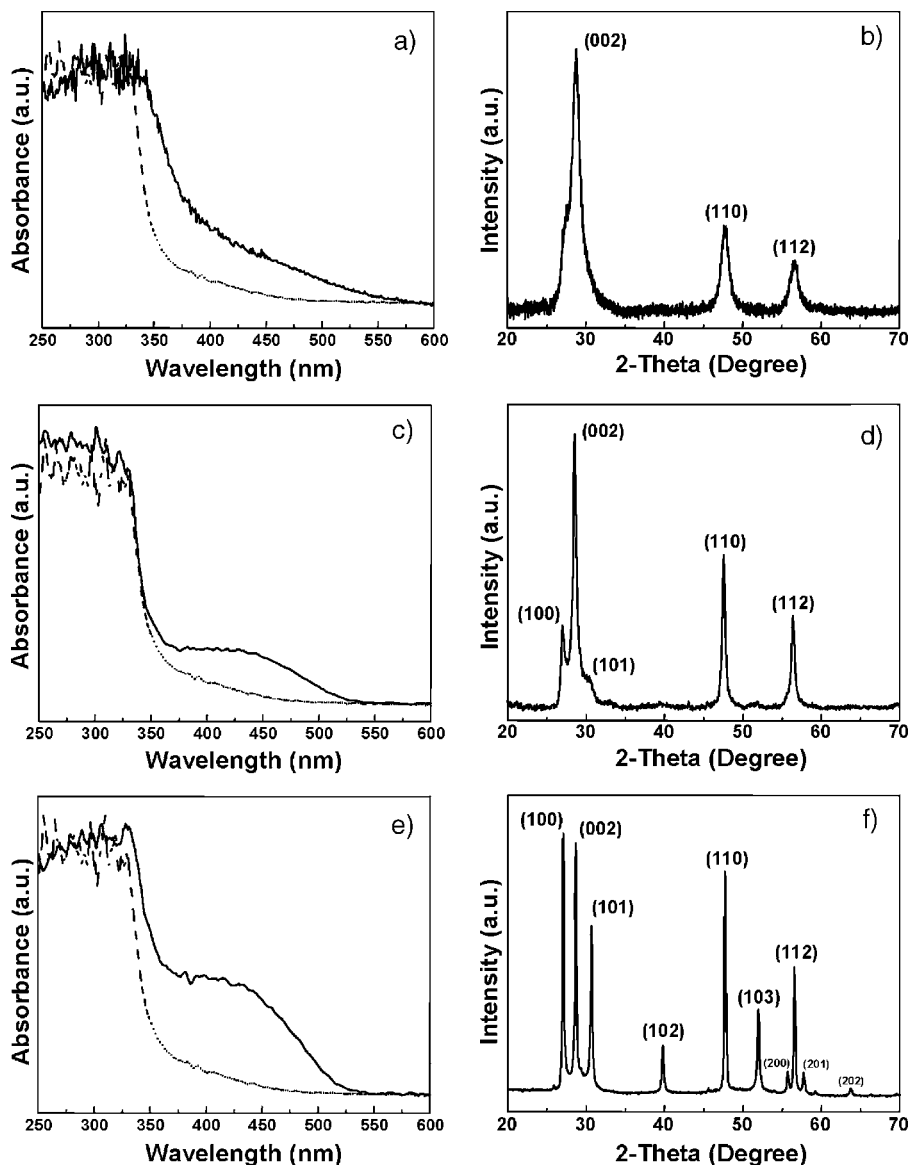


Figure 3. Diffuse reflectance UV-vis spectra and XRD patterns of USP-prepared ZnS:Ni²⁺ hollow microspheres (a and b, respectively), nanoparticles (c and d, respectively), and non-templated solid microspheres (e and f, respectively). For comparison, the diffuse reflectance UV-vis spectrum of pure ZnS powder is given as a dashed line in (a), (c), and (e).

smaller surface area: too many photo-excitations do not lead to surface accessible redox. These results emphasize the balance needed between crystallinity and surface area of a photocatalyst for an optimal high activity.^[10]

For comparison to our USP nanoparticles, we also prepared ZnS:Ni²⁺ powders using the traditional co-precipitation method, as previously reported by Kudo et al.^[2c] Figure 5b shows that the photocatalytic activity of the USP nanoparticles for H₂ production is substantially superior to those of ZnS:Ni²⁺ powders obtained from the co-precipitation method (see Figs. S11 and 12 in SI for characterization of the co-precipitation powders). In addition, the USP nanoparticles did not show deactivation during the photocatalytic reaction, which reveals the improved stability of the USP nanoparticles compared to the ZnS:Ni²⁺ powders. The quantum efficiency of the USP nanoparticles at 430 nm was found to be (2.1 ± 0.2)%, which is much higher than the quantum efficiency reported by Kudo et al. (1.3% at 420 nm).^[2c] While the co-precipitation method is simple and easy (especially for small scale preparations), it has severe limitations in the preparation of highly active photocatalysts that are well-balanced between crystallinity and surface area. Our results clearly demonstrate that USP is a robust and efficient method to achieve the requirement of a highly active photocatalyst.

In conclusion, nanostructured ZnS:Ni²⁺ hollow microspheres and

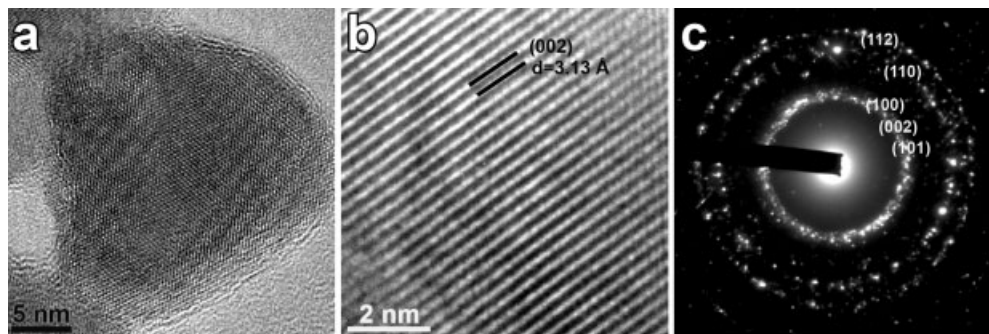


Figure 4. a,b) High-resolution TEM images and c) SAED pattern of ZnS:Ni²⁺ nanoparticles prepared by USP.

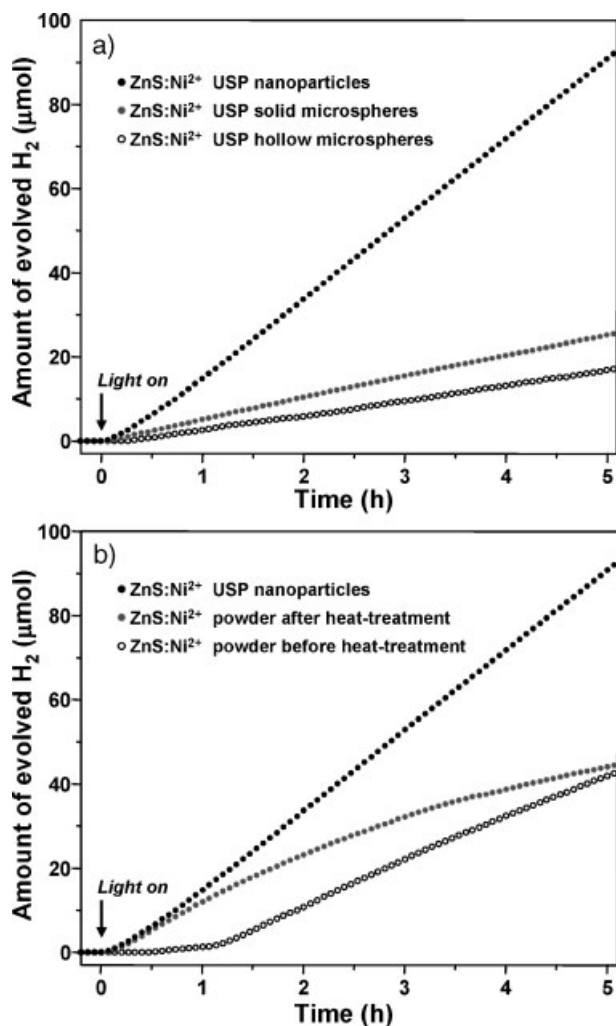


Figure 5. a) Photocatalytic activities for H₂ production of USP-prepared ZnS:Ni²⁺ nanoparticles, solid microspheres, and hollow microspheres under visible light irradiation ($\lambda > 400$ nm). b) Photocatalytic activities under visible light irradiation ($\lambda > 400$ nm) of ZnS:Ni²⁺ nanoparticles prepared by USP, as-obtained ZnS:Ni²⁺ powder prepared by traditional co-precipitation, and heat-treated ZnS:Ni²⁺ co-precipitated powder (500 °C, 2 h under Ar flow). In each case, 0.1 g of a photocatalyst was suspended in 50 mL of an aqueous solution (0.5 M K₂SO₃, 5 mM Na₂S).

nanoparticles have been prepared using USP. Their morphology was easily controlled by changing reaction temperatures, and the photocatalytic activity of ZnS:Ni²⁺ nanoparticles for H₂ production was substantially superior to those of ZnS:Ni²⁺ hollow spheres and solid spheres due to their good crystallinity and high surface area. Also, we find that the USP nanoparticles are significantly more active and stable than ZnS:Ni²⁺ powders prepared by traditional co-precipitation, demonstrating the usefulness of USP as a robust synthetic approach to prepare highly active photocatalysts. We believe that ultrasonic spray pyrolysis will be easily generalized for the preparation of other nanostructured metal sulfide and oxide photocatalysts.

Experimental

The aqueous ZnS precursor solution was 200 mM zinc nitrate, 1 M thiourea, and 0.2 mM nickel nitrate (i.e., 0.1 atomic wt % versus Zn) and prepared from reagent grade materials used as purchased. The precursor solution will begin to form a precipitate after ca. 24 h, but the precipitate will quickly redissolve or re-suspend upon being shaken. 3 ml of colloidal silica (Sigma–Aldrich; Ludox TMA, 34 wt % of silica suspended in water, particle diameter ~23 nm) was added to 47 ml of the ZnS precursor solution. The resulting solution was introduced into an atomization cell and nebulized by a 1.7 MHz household ultrasonic humidifier (Sunbeam model 696). Aerosols produced by the nebulization were carried through a furnace by Ar gas flow at a rate of 1.0 standard liter per minute (SLPM). The furnace temperature was set either to 700 °C for hollow microsphere synthesis or to 1000 °C for nanoparticle synthesis. The product was collected in a series of several bubblers containing deionized water and then isolated from the collection media by centrifugation. After washing and centrifuging the product with deionized water several times, it was re-dispersed in 10% HF in ethanol to leach out the silica templates and left at room temperature for 24 h. The resulting product was centrifuged, washed several times with ethanol and water, and dried at room temperature.

As a control experiment, ZnS:Ni²⁺ powder was prepared using a co-precipitation method, as previously reported [2c]. Aqueous sodium sulfide solution (1 M, 50 ml) and zinc nitrate solution (0.2 M, 100 ml) containing 0.2 mM nickel nitrate were mixed together and stirred for 15 h at room temperature. The obtained precipitate was washed thoroughly with deionized water several times and dried under room temperature. The dried powder was placed in a quartz tube for 2 h under Ar flow to completely remove oxygen from the tube and then heat-treated at 500 °C under Ar flow for 2 h to improve the crystallinity.

For characterization, scanning electron microscopy (SEM) was carried out with a Hitachi S-4700, and transmission electron microscopy (TEM) was conducted with a JEOL 2010F. Diffuse reflectance UV-vis spectra of the products were obtained using a Hitachi 3300 double monochromator UV-vis spectrophotometer, and powder X-ray diffraction (XRD) patterns were taken with a Rigaku D-MAX diffractometer using a Cu K α radiation. Nitrogen adsorption and desorption isotherms were measured with a Nova 2200e Surface Area and Pore Analyzer (Quantachrome Instruments) at liquid nitrogen temperature (–196 °C), and the specific surface areas were determined by the BET method. The pore size distribution of ZnS:Ni²⁺ hollow microspheres was analyzed using the Barrett–Joyner–Halenda (BJH) method with the adsorption branch [11]. Photocatalytic activity of ZnS:Ni²⁺ photocatalysts towards water-splitting was evaluated under visible light in an aqueous solution containing 0.5 M K₂SO₃ and 5 mM Na₂S as hole scavengers, as previously noted [2c]. In each case, 0.1 g of ZnS:Ni²⁺ powder was dispersed in an aqueous solution (50 mL) containing K₂SO₃ (0.5 M) and Na₂S (5 mM) and introduced into a water-jacketed quartz cell with a magnetic stir bar. ZnS:Ni²⁺ photocatalyst was then irradiated with visible light ($\lambda > 400$ nm) from a 300 W Xe lamp passed through a 2 M aqueous NaNO₂ long-pass optical filter (see Fig. S13 in SI for a transmission spectrum of the filter solution). ZnS:Ni²⁺ powder was kept stirred with a magnetic stir bar, and the quartz cell was cooled with circulating water to prevent heating. The amount of evolved H₂ gas was monitored with a gas chromatography (GC) equipped with a thermal conductivity detector (Agilent 6890 GC, G1532-60720 TCD). The quantum efficiency (QE) of H₂ production by ZnS:Ni²⁺ nanoparticles was calculated using the follow equation:

$$Q.E. (\%) = \frac{\text{number of evolved H}_2 \text{ molecules} \times 2}{\text{number of incident photons}} \times 100$$

where the number of incident photons at 430 nm was measured using a band pass filter ($\lambda_{\text{max}} = 430$ nm, half width = 10 nm) and chemical

actinometry using potassium ferrioxalate; all photons were assumed to be absorbed by the photocatalyst (i.e., light scattering ignored: the QE is therefore a lower limit) [12].

Received: December 23, 2007

Revised: January 18, 2008

Published online: May 29, 2008

- [1] a) A. Wolosiuk, O. Armagan, P. V. Braun, *J. Am. Chem. Soc.* **2005**, *127*, 16356. b) B. Xia, I. W. Lenggoro, K. Okuyama, *Chem. Mater.* **2002**, *14*, 4969. c) J.-S. Hu, L.-L. Ren, Y.-G. Guo, H.-P. Liang, A.-M. Cao, L.-J. Wan, C.-L. Bai, *Angew. Chem. Int. Ed.* **2005**, *44*, 1269. d) Q. Zhao, Y. Xie, Z. Zhang, X. Bai, *Cryst. Growth Des.* **2007**, *7*, 153. e) I. D. Hosein, C. M. Liddell, *Langmuir* **2007**, *23*, 2892. f) Z. Quan, Z. Wang, P. Yang, J. Lin, J. Fang, *Inorg. Chem.* **2007**, *46*, 1354.
- [2] a) X. Wang, S. O. Pehkonen, A. K. Ray, *Ind. Eng. Chem. Res.* **2004**, *43*, 1665. b) H. Yin, Y. Wada, T. Kitamura, S. Yanagida, *Environ. Sci. Technol.* **2001**, *35*, 227. c) A. Kudo, M. Sekizawa, *Chem. Commun.* **2000**, 1371. d) A. Kudo, M. Sekizawa, *Catal. Lett.* **1999**, *58*, 241. e) I. Tsuji, A. Kudo, *J. Photochem. Photobiol. A* **2003**, *156*, 249.
- [3] a) N. Kumbhojkar, V. V. Nikesh, A. Kshirsagar, S. Mahamuni, *J. Appl. Phys.* **2000**, *88*, 6260. b) H. Tong, Y.-J. Zhu, L.-X. Yang, L. Li, L. Zhang, J. Chang, L.-Q. An, S.-W. Wang, *J. Phys. Chem. C* **2007**, *111*, 3893. c) W.-T. Yao, S.-H. Yu, Q.-S. Wu, *Adv. Funct. Mater.* **2007**, *17*, 623.
- [4] a) M. T. Swihart, *Curr. Opin. Colloid Interface Sci.* **2003**, *8*, 127. b) K. Okuyama, M. Abdullah, I. W. Lenggoro, F. Iskandar, *Adv. Powder Technol.* **2006**, *17*, 587. c) T. T. Kodas, M. J. Hampden-Smith, *Aerosol Processing of Materials*, Wiley, New York **1999**.
- [5] a) S. E. Skrabalak, K. S. Suslick, *J. Am. Chem. Soc.* **2005**, *127*, 9990. b) Y. Didenko, K. S. Suslick, *J. Am. Chem. Soc.* **2005**, *127*, 12196.
- [6] a) J. E. Hampsey, Q. Y. Hu, L. Rice, J. B. Pang, Z. W. Wu, Y. F. Lu, *Chem. Commun.* **2005**, 3606. b) W. H. Suh, K. S. Suslick, *J. Am. Chem. Soc.* **2005**, *127*, 12007. c) J. E. Hampsey, S. Arsenault, Q. Hu, Y. Lu, *Chem. Mater.* **2005**, *17*, 2475. d) A. Prakash, A. V. McCormick, M. R. Zachariah, *Nano Lett.* **2005**, *5*, 1357. e) W. H. Suh, A. R. Jang, Y.-H. Suh, K. S. Suslick, *Adv. Mater.* **2006**, *18*, 1832. f) X. Jiang, C. J. Brinker, *J. Am. Chem. Soc.* **2006**, *128*, 4512. g) S. E. Skrabalak, K. S. Suslick, *J. Am. Chem. Soc.* **2006**, *128*, 12642. h) T. Zheng, J. Zhan, J. Pang, G. S. Tan, J. He, G. L. McPherson, Y. Lu, V. T. John, *Adv. Mater.* **2006**, *18*, 2735. i) F. Iskandar, A. B. D. Nandiyanto, K. M. Yun, C. J. Hogan, K. Okuyama, P. Biswas, *Adv. Mater.* **2007**, *19*, 1408. j) J. H. Bang, K. Han, S. E. Skrabalak, H. Kim, K. S. Suslick, *J. Phys. Chem. C* **2007**, *111*, 10959.
- [7] Q. Wu, H. Cao, S. Zhang, X. Zhang, D. Rabinovich, *Inorg. Chem.* **2006**, *45*, 7316.
- [8] a) J.-H. Lee, S.-J. Park, *J. Am. Ceram. Soc.* **1993**, *76*, 777. b) G. L. Messing, S.-C. Zhang, G. V. Jayanthi, *J. Am. Ceram. Soc.* **1993**, *76*, 2707. c) K. Okuyama, I. W. Lenggoro, *Chem. Eng. Sci.* **2003**, *58*, 537.
- [9] a) D. Jing, L. Guo, *J. Phys. Chem. B* **2006**, *110*, 11139. b) I. Tsuji, H. Kato, H. Kobayashi, A. Kudo, *J. Am. Chem. Soc.* **2004**, *126*, 13406. c) I. Tsuji, H. Kato, A. Kudo, *Angew. Chem. Int. Ed.* **2005**, *44*, 3565.
- [10] a) M. Kaneko, I. Okura, *Photocatalysis*, Springer, New York **2002**. b) A. Kudo, H. Kato, I. Tsuji, *Chem. Lett.* **2004**, 1534. c) J. S. Lee, *Catal. Surv. Asia* **2005**, *9*, 217. d) K. Maeda, K. Domen, *J. Phys. Chem. C* **2007**, *111*, 7851. e) F. E. Osterloh, *Chem. Mater.* **2008**, *20*, 35.
- [11] E. P. Barrett, L. G. Joyner, P. P. Halenda, *J. Am. Chem. Soc.* **1951**, *73*, 373.
- [12] J. G. Calvert, J. N. Pitts, Jr., *Photochemistry*, Wiley, New York **1966**.